Investigation of PCB-based Inductive Sensors Orientation for Corona Partial Discharge Detection

Antonino Imburgia
Department of Engineering
University of Palermo
Palermo, Italy
antonino.imburgia01@unipa.it

Sinda Kaziz
Faculty of Sciences of Monastir,
University of Monastir,
Monastir, Tunisia
sinda.kaziz@fsm.u-monastir.tn

Pietro Romano
Department of Engineering
University of Palermo
Palermo, Italy
pietro.romano@unipa.it

Denis Flandre
ICTEAM Institute
Université catholique de Louvain
Louvain-la-Neuve, Belgium
denis.flandre@uclouvain.be

Giovanni Artale
Department of Engineering
University of Palermo
Palermo, Italy
giovanni.artale@unipa.it

Giuseppe Rizzo
Prysmian Electronics
Prysmian Group
Palermo, Italy
giuseppe.rizzo@prysmiangroup.com

Fabio Viola
Department of Engineering
University of Palermo
Palermo, Italy
fabio.viola@unipa.it

Fares Tounsi
ICTEAM Institute
Université catholique de Louvain
Louvain-la-Neuve, Belgium
fares.tounsi@uclouvain.be

Guido Ala
Department of Engineering
University of Palermo
Palermo, Italy
guido.ala@unipa.it

2022 IEEE 21st Mediterranean Electrotechnical Conference (MELECON) | 978-1-6654-4280-0/22/$31.00 ©2022 IEEE | DOI: 10.1109/MELECON53508.2022.9843026

***Abstract*—This paper presents an experimental investigation of two different printed circuit board (PCB) inductive sensors, with meander and non-spiral shapes, to assess their capabilities and best orientation for corona partial discharge (PD) detection. First, simulations with the Ansys HFSS software are performed in order to evaluate the equivalent electrical circuit of the two sensors and their 2d radiation patterns. The meander sensors presented a resonant frequency of 600 MHz, while it was around 1.1 GHz for the non-spiral. The 2d radiation pattern showed that better sensitivity is achieved when the inductive sensor is oriented 90 degrees with respect to the PD source. Experimental tests showed a peak-to-peak voltage of the PD signal detected by both sensors of around 14 mV when the orientation was 90 degrees with a main frequency around 35 MHz. The peak-to-peak voltage dropped to about 5.4 mV and 6.9 mV for the meander and the non-spiral sensors, respectively, with a main frequency of about 33.5 MHz, when the orientation was 0 degrees. The obtained PRPD patterns and the PD signal shapes were quite similar to those provided by a High-Frequency Current Transformer (HFCT) commercial sensor.**

Keywords—inductive loop, PCB-based sensor, planar inductors, partial discharge detection.

I. Introduction

The stability of any power system network is determined mainly by the high-voltage equipment used. Failure of this equipment is chiefly related to partial discharge (PD) phenomena. Measurements of PD are one of the most common monitoring techniques used in medium and high-voltage electrical grids. This type of measurement, in particular, gives valuable information on the operational status evaluation of cables, joints, terminations, and other components used in high voltage systems [1]. PD is a breakdown that occurs in a part of the insulating material caused by an overly high electric field. Since it is a widely accepted signal for defects, it is widely utilized in power equipment testing and diagnostics. PD can occur wherever there is an insulation defect, from solid- to oil- or gas-insulated equipment [2]. Early diagnosis of PD is critical because it can avoid more significant damage to high-voltage equipment. When the PD is recognized, issues can be anticipated, and preventative maintenance can begin earlier [3]. Various methods can be used to detect PD, such as electrical methods, chemicals, acoustics, optics, and electromagnetic methods. In the last few years, several types of sensors have been developed, taking advantage of the electromagnetic waves produced during PD pulses. Electromagnetic (EM) radiation contains a combination of different frequency components up to a few GHz, falling within the low microwave band (HF, VHF, and UHF bands) [2]. EM radiation can be detected using UHF/VHF antennas, VHF capacitive couplers, or inductive sensors such as High Frequency Current Transformer (HFCT) sensors [4], Inductive Loop Sensors (ILSs) [5], on-chip loop antennas [2], and Rogowski Coil (RC) sensors [5]. EM detection sensors permit non-contact measurements and provide good isolation between the measurement equipment and the sensor. In recent years, various antenna sensors have been developed to detect PD in different applications. The antenna sensor described in [6] is used to measure the PD in power transformers, whereas the antenna sensor suggested in [7] is employed in metal-enclosed switchgear. Instead, UHF, optical, and HFCT PD probes are utilized to monitor PD in Gas-Insulated Switchgear (GIS) [8], [9]. In comparison to the previous reported PD antennas, which are utilized in very specialized contexts due to their design features, the PD sensors evaluated in this work, primarily designed to detect PD on transformers, are based on a general-purpose measuring system capable of detecting PD signals in a variety of application domains.

In this paper, two PCB-based inductive sensors are studied and analyzed to be used in PD detection. Thereupon, two different coil topologies are evaluated using the Ansys HFSS (High-Frequency Structure Simulator) software based on the Finite Element Method (FEM). The experimental setup for partial discharge generation, as well as the results of the antenna measurements, are presented. This paper also confronts the performance of each structure to identify the best sensitivity towards PD pulses and then compares the results with a common industrial sensor. Finally, the sensor responses are analyzed according to different directions and distances from the PD source.

II. Antenna Design and Evaluation

A. Antenna design and fabrication

Two different planar inductive sensor topologies, shown in Fig. 1, are designed in this work to be evaluated. The two topologies, i.e., the non-spiral (Fig. 1.a) and the meander (Fig. 1.b), belong to the single-layer inductor category. Single-layer types have the entire layout and the two contact pads on the same level, so only one metal layer during fabrication is required [10]. Hence, there is no need for an internal metal pad contact as in a two-layer loop spiral sensor. The two sensors are made on an FR-4 substrate with a thickness of 1.7 mm and a relative dielectric constant of 4.4. Table 1 lists their geometric dimensions, where D and d are the outer and inner diameters, respectively, n is the turns number, and w and s are the track width and spacing, respectively. The two fabricated structures have the same external dimensions of 20×20 mm^2. This type of inductive sensor presents various advantages over conventional ones since it is small, simple, low cost, and does not require an external power supply. In addition, it can be placed close to the source of the PD in order to increase its sensitivity.

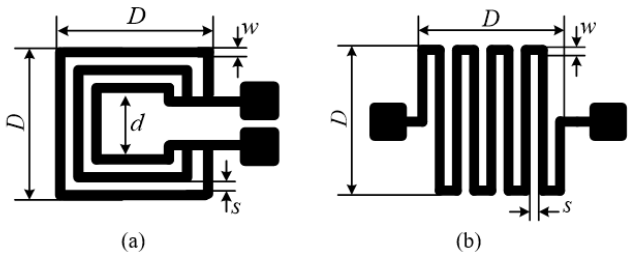

Fig. 1. Evaluated inductive sensor topologies: (a) non-spiral, (b) meander.

Table 1. Different planar inductive sensor dimensions values

Parameter	*n*	*D*	*d*	*w*	*s*
Value (mm)	6.5	20	5.2	0.4	0.4

B. HFSS simulation results

HFSS software is commonly used for modelling electromagnetic structures and determining their high-frequency behavior. The HFSS graphical user interface (GUI) in Fig. 2 depicts the meander topology inductive sensor mounted on an FR-4 substrate and surrounded by an air box. The simulated impedance modules and phase angles of the meander and non-spiral inductive sensors are shown in Fig. 3 and Fig. 4, respectively. As can be observed, the meander sensor exhibits a first self-resonance frequency (SRF) of about 600 MHz, while the non-spiral inductor shows a first self-resonance frequency of 1.1 GHz. The phase angle is 90 degrees for frequencies less than 600 MHz for the meander sensor and 1.1 GHz for the non-spiral sensor. Accordingly, the two structures will behave inductively until they reach their characteristic resonance frequency, at which point they will behave capacitively.

Radiation patterns in the loop plane versus frequency simulations for both inductive sensors have been drawn with the aim of investigating the best orientation of each of the topologies. Figs. 5 and 6 show, respectively, the two-dimensional (2d) radiation patterns of the meander and the non-spiral sensor at frequencies varying from 10 MHz to

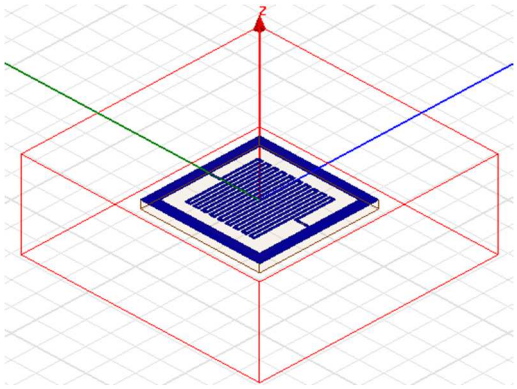

Fig. 2. Meander topology inductive sensor designed in HFSS.

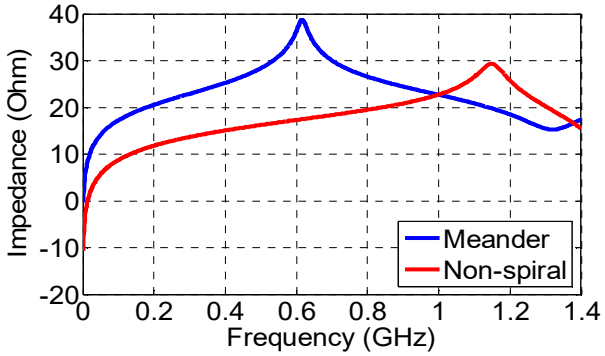

Fig. 3. Simulated impedance modules of the meander and non-spiral inductive sensors.

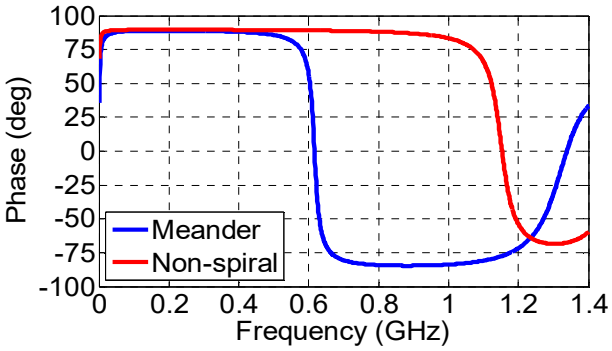

Fig. 4. Simulated phase angles of the meander and the non-spiral inductive sensors.

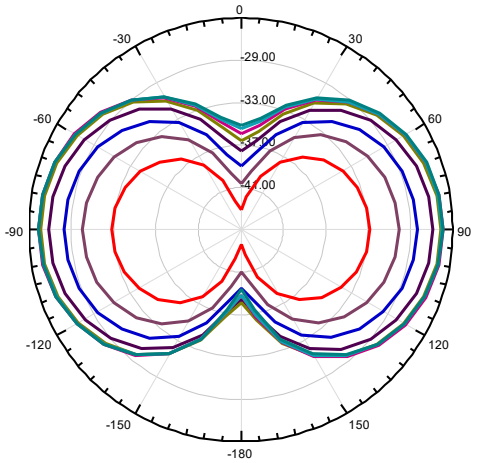

Fig. 5. Simulation results of the 2d radiation pattern (directivity in the loop plane) of the meander sensor at frequencies varying from 10 MHz to 45 MHz with 5 MHz increments (the internal curve corresponds to the 10 MHz).

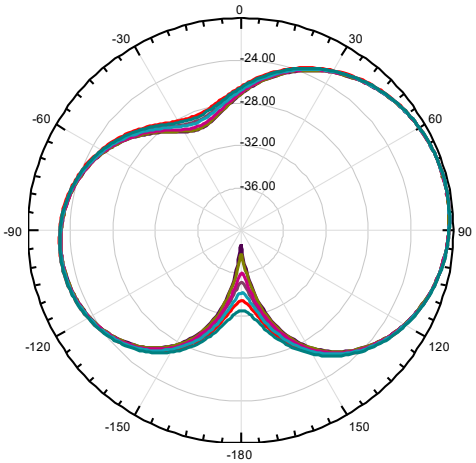

Fig. 6. Simulation results of the 2d radiation pattern (directivity in the loop plane) of the non-spiral sensor at frequencies varying from 10 MHz to 45 MHz with 5 MHz increments (the internal curve corresponds to the 10 MHz).

45 MHz with an increment of 5 MHz. The simulated radiation patterns are made for frequencies below the resonant frequency of the sensors and in the vicinity of the expected PD frequencies. Contrary to the self-resonant loop antennas, the radiation and reception pattern of small loops peaks within the plane of the loop rather than broadside to it [11]. Hence, both simulated sensors showed maximum radiation or reception capacities when they were oriented at an angle of 90 degrees with respect to the PD source. This is due to the changes in the effective area crossed by the emitted magnetic field, as stated by Faraday's law of induction. This law explains, as well, the lower sensor performance at low frequencies. Hence, when the sensor operates at a low frequency, the reception area is located mostly at its edge. As the frequency increases, the radiation reception pattern becomes on the broadside, which is near the center of the sensor.

III. Measurement Setup

For the corona PD tests, the adopted measurement setup is shown in Fig. 7. There is a high voltage generator, a corona PD source in the typical needle-to-plane specimen configuration, the board printed antennas, and the PryCam Grids. The sensor is connected to the PryCam by means of a BNC cable, while the PD signal is sent to the computer by means of an optical fiber connection. The distance between the corona PD source and the sensor has been chosen to be equal to 9 cm. This is to avoid the occurrence of discharges between the needle and the antenna itself.

IV. PD Measurement Results

PD tests have been conducted for both sensors at the same measurement conditions. The magnitude of the applied voltage was 3 kV, which corresponds to the Partial Discharge Inception Voltage (PDIV). In order to compare performance towards PD detection between the two types of PCB-based sensors and the HFCT sensor, the obtained PRPD (Phase-resolved partial discharge) patterns are analyzed. They are reported in Fig. 9, where Fig. 9a is related to the meander, Fig. 9c to the non-spiral sensor, and Fig. 9c to the HFCT sensor. In order to generate statistically significant results, approximately 3000 corona PD pulses (black dots in Fig. 9) were acquired in the experiment. All the above-reported figures related to the PRPD pattern, the detected PD pulse, and the frequency spectrum have been provided by the PryCam Grids acquisition software.

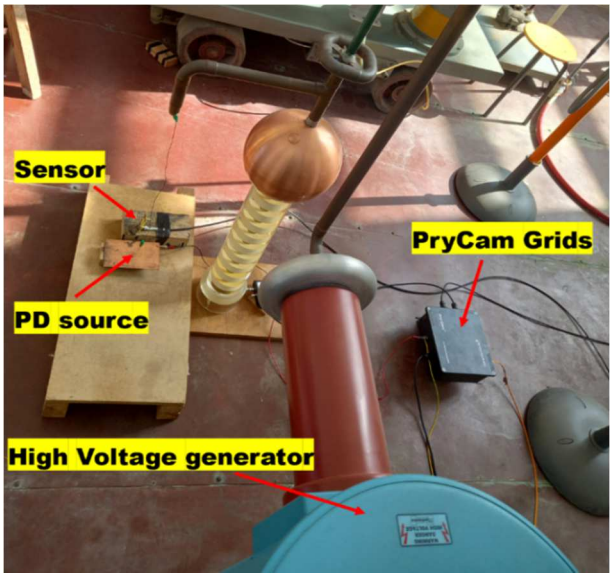

Fig. 7. PD measurement setup.

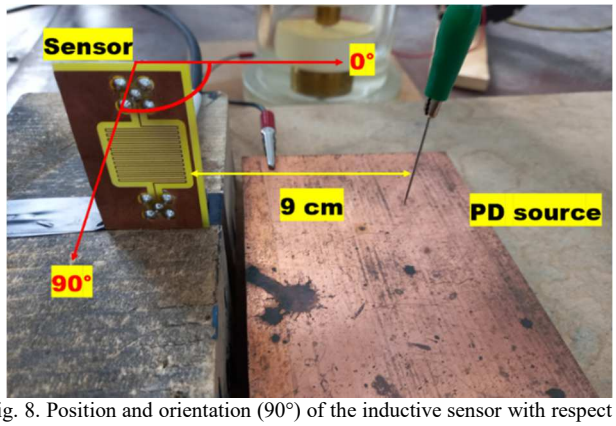

Fig. 8. Position and orientation (90°) of the inductive sensor with respect to the corona PD source.

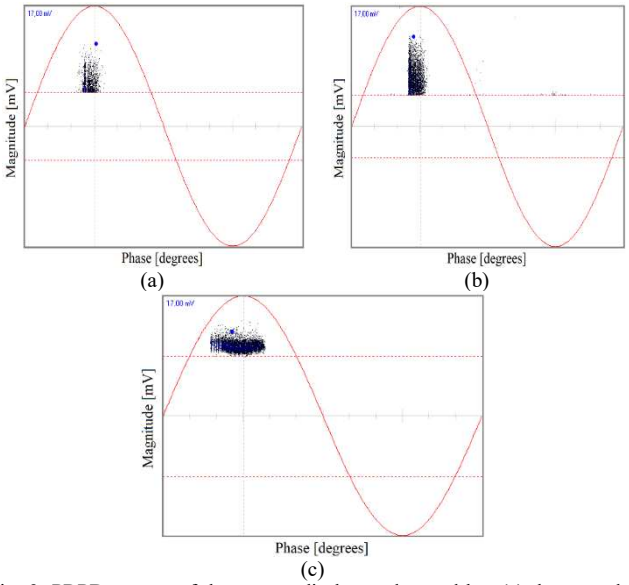

Fig. 9. PRPD pattern of the corona discharge detected by: (a) the meander inductive sensor, (b) the non-spiral inductive sensor, and (c) the HFCT sensor.

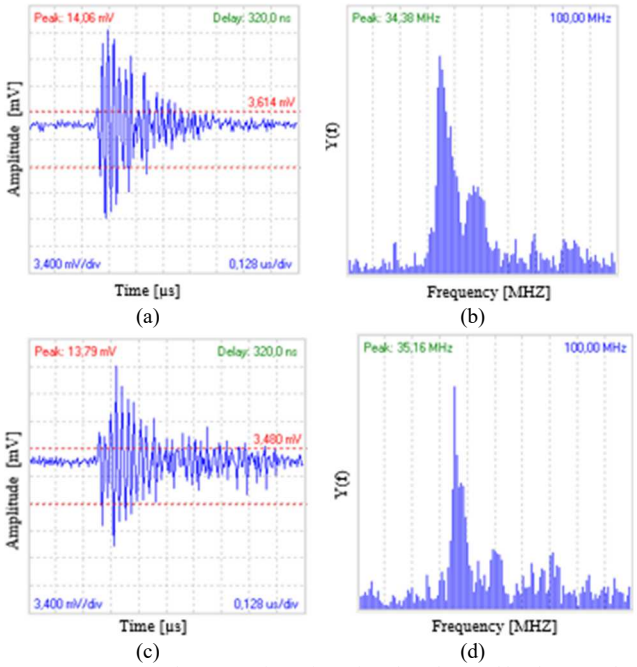

Fig. 10. Corona PD pulse at an orientation of 90 deg. detected by the meander inductor sensor in (a) and its frequency spectrum in (b), corona PD pulse detected by the non-spiral sensor in (c) and its frequency spectrum in (d).

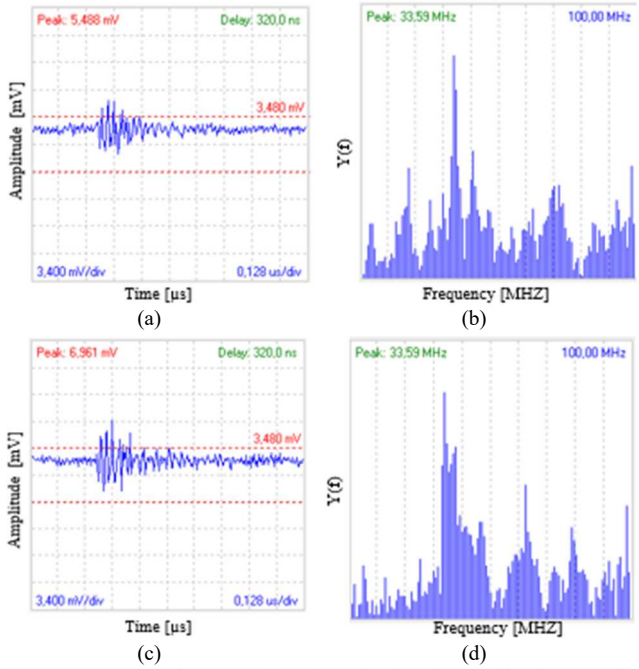

Fig.11. Corona PD pulse at an orientation of 0 deg. detected by the meander inductor sensor in (a) and its frequency spectrum in (b), corona PD pulse detected by the non-spiral sensor in (c) and its frequency spectrum in (d).

The detected PD pulses from the meander and the non-spiral inductive sensors are depicted in Figs. 10a and 10c, respectively, taken at an angle of 90 degrees with respect to the PD source. Figs. 10b and 10d present the spectrum frequency of the pulse signals issued from the meander and non-spiral sensor, respectively. As can be seen, the magnitudes of the pulses of the discharges acquired by both sensors are very comparable, which were 14.06 mV and 13.97 mV, from the meander and the non-spiral, respectively. For both examined sensors, the frequency spectrum shows a maximum peak of around 35 MHz.

Figs. 11a and 11b illustrate the corona PD signal pulses detected by the meander and the non-spiral sensor when they are placed at an angle of 0 degree with respect to the PD source. As can be observed, the peak-to-peak voltage of the PD signal detected by the meander inductor is 5.4 mV, while 6.9 mV is detected by the non-spiral sensor. It is worth remembering that, as expected from Figs. 5 and 6, the maximum PD signal magnitude was better sensed by the sensor when it was placed at 90 degrees with respect to the PD source. Figs. 11b and 11d present the spectrum frequency of the pulse signal of the meander sensor and the non-spiral sensor, respectively. The two sensors present the same maximum amplitude of the fundamental lobe of the PD signal at the frequency of 35.59 MHz. It can be highlighted, that the meander inductive sensor has a lower attenuation in the lower frequency range when it is oriented at 0 degrees.

Both the PRPD pattern and the single PD pulse show some differences compared to those typically provided by a commercial HFCT PD sensor. In Figs. 12a and 12b, the single PD pulse and the related frequency spectrum, are reported, respectively. As can be observed these figures, the HFCT sensor mainly detects PD pulses of lower frequencies, which is a typical signal feature of corona discharges. With the HFCT the frequency spectrum shows a maximum amplitude equal to 2.3 MHz, while the magnitude of the

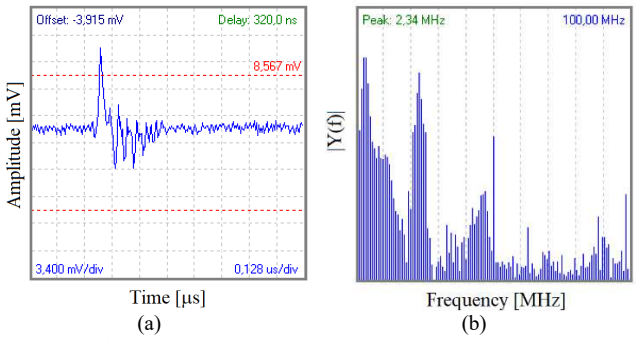

Fig. 12. Single corona PD pulse detected by HFCT sensor in (a) and its frequency spectrum in (b).

detected discharge signals is around 12 mV which is comparable to the found signals.

In the present work, for the comparison with the board-printed sensors, an HFCT sensor has been used. However, the investigated sensors were designed to detect PD signals with high-frequency content, e.g., PD within transformers or gas-insulated switchgears (GIS). Therefore, the best efficiency of these inductive sensors is given for the detection of PD signals with frequency bands in the order of GHz. While the PD pulses in our experimental test have lower frequency content, with a band in the order of MHz. In future work, with the aim of obtaining a detected PD signal and associated frequency spectrum similar to that typical provided by commercial sensors, the study will focus on changes in the geometric dimensions of the sensors as well as their shape.

V. Conclusion

In the proposed work, the performance towards PD detection of two different printed-board sensors, named meander and non-spiral, has been investigated. First, simulations by means of HFSS software have been conducted in order to analyze the impedance modules and phase angles of each sensor. According to the simulations, the meander

inductive sensors showed a first resonant frequency of 600 MHz and 1.1 GHz for the non-spiral inductive sensor. The 2d radiation pattern was also simulated. It has been found that for best sensitivity, the inductive sensor should be placed at a 90-degrees angle to the DP source. At this orientation, the maximum discharge magnitude values detected by the two investigated sensors were similar and around 14.06 mV. The frequency spectrum showed a maximum amplitude of 34.8 MHz with the meander inductor and 35.16 MHz with the non-spiral inductor. These latter values are slightly higher than typical values obtained from commercial HFCT sensors. Future work will also be dedicated to in-depth characterization of the influence of the geometric parameters of the meander and non-spiral sensors.

REFERENCES

[1] J. Smit, E. Gulski, and F. Wester, "Economical and technical aspects of advanced PD diagnostics to support condition based maintenance of HV assets," in IEEE/PES Transmission and Distribution Conference and Exhibition, vol. 2, pp. 1110–1115, 2002.

[2] N. Zeidi, S. Kaziz, M. H. Said, L. Rufer, A. Cavallini, and F. Tounsi, "Partial discharge detection with on-chip spiral inductor as a loop antenna," Review of Scientific Instruments, vol. 92, no. 9, p. 094701, 2021.

[3] A. Cavallini, G. C. Montanari, M. Tozzi, and X. Chen, "Diagnostic of HVDC systems using partial discharges," IEEE Transactions on Dielectrics and Electrical Insulation, vol. 18, no. 1, pp. 275–284, 2011.

[4] F. Álvarez, F. Garnacho, J. Ortego, and M. Á. Sánchez-Urán, "Application of HFCT and UHF sensors in on-line partial discharge measurements for insulation diagnosis of high voltage equipment," Sensors, vol. 15, no. 4, pp. 7360–7387, 2015.

[5] M. Argüeso, G. Robles, and J. Sanz, "Implementation of a Rogowski coil for the measurement of partial discharges," Review of scientific instruments, vol. 76, no. 6, p. 065107, 2005.

[6] J. Lopez-Roldan, T. Tang, and M. Gaskin, "Optimisation of a sensor for onsite detection of partial discharges in power transformers by the UHF method," IEEE Transactions on Dielectrics and Electrical Insulation, vol. 15, no. 6, pp. 1634–1639, 2008.

[7] C. Zhang, M. Dong, M. Ren, W. Huang, J. Zhou, X. Gao, and R. Albarracín, "Partial discharge monitoring on metal-enclosed switchgear with distributed non-contact sensors," Sensors, vol. 18, no. 2, p. 551, 2018.

[8] X. Han, J. Li, L. Zhang, P. Pang, and S. Shen, "A novel PD detection technique for use in GIS based on a combination of UHF and optical sensors," IEEE Transactions on Instrumentation and Measurement, vol. 68, no. 8, pp. 2890–2897, 2018.

[9] A. Rodrigo Mor, L. C. Castro Heredia, and F. A. Muñoz, "A novel approach for partial discharge measurements on GIS using HFCT sensors," Sensors, vol. 18, no. 12, p. 4482, 2018.

[10] S. Kaziz, B. Maamer, T. Delhaye, F. Tounsi, L. A. Francis, and D. Flandre, "Tuning Range Comparison Between Different Planar Inductors Layouts on PCB," in IEEE International Conference on Design & Test of Integrated Micro & Nano-Systems (DTS), pp. 1–6, 2020.

[11] C. A Balanis, "Antenna Theory: Analysis and Design," 4th edition, John Wiley & Sons (ISBN: 978-1-118-64206-1), 2016.

FUNDING ACKNOWLEDGEMENT

This work was carried out with support received from the European Union's Horizon 2020 research and innovation program under the Marie Skłodowska-Curie individual fellowship agreement No. 101030887.

CITATION AND KEYWORDS

Antonino Imburgia, Sinda Kaziz, Pietro Romano, Denis Flandre, Giovanni Artale, Giuseppe Rizzo, Fabio Viola, Fares Tounsi, and Guido Ala, "Investigation of PCB-based Inductive Sensors Orientation for Corona Partial Discharge Detection," IEEE 21st International Mediterranean Electrotechnical Conference (MELECON'22), Palermo, Italy, 2022, pp. 559-563, doi: 10.1109/MELECON53508.2022.9843026..

Keywords: {Inductive loop, PCB-based sensor, Planar inductors, Partial discharge detection},